Properties of light particles produced in Ar+Ni collisions at 95*A* MeV: Prompt emission and evaporation

D. Doré,[1] C. Volant,[1] J. Cugnon,[2] R. Legrain,[1,*] G. Auger,[3] Ch. O. Bacri,[4] N. Bellaize,[5] B. Borderie,[4] R. Bougault,[5] B. Bouriquet,[3] R. Brou,[5] P. Buchet,[1] J. L. Charvet,[1] A. Chbihi,[3] J. Colin,[5] D. Cussol,[5] R. Dayras,[1] A. Demeyer,[6] D. Durand,[5] J. D. Frankland,[3] E. Galichet,[4,9] E. Genouin-Duhamel,[5] E. Gerlic,[6] D. Guinet,[6] B. Guiot,[3] S. Hudan,[3] P. Lautesse,[6] F. Lavaud,[4] J. L. Laville,[3] J. F. Lecolley,[5] C. Leduc,[6] N. Le Neindre,[5] O. Lopez,[5] M. Louvel,[5] A. M. Maskay,[6] L. Nalpas,[1] J. Normand,[5] P. Pawłowski,[4] M. Pârlog,[7] E. Plagnol,[4] M. F. Rivet,[4] E. Rosato,[8] F. Saint-Laurent,[3,†] J. C. Steckmeyer,[5] G. Tăbăcaru,[7] B. Tamain,[5] L. Tassan-Got,[4] E. Vient,[5] and J. P. Wieleczko[3]

(INDRA Collaboration)

[1]*DAPNIA/SPhN, CEA/Saclay, F-91191 Gif-sur-Yvette Cedex, France*
[2]*University of Liège, Physics Department, B5, B-4000 Sart-Tilman Liège 1, Belgium*
[3]*GANIL (DSM-CEA/IN2P3-CNRS), B.P. 5027, F-14076 Caen Cedex 5, France*
[4]*IPN Orsay (IN2P3-CNRS), F-91406 Orsay Cedex, France*
[5]*LPC Caen (IN2P3-CNRS/ISMRA et Université), F-14050 Caen Cedex, France*
[6]*IPN Lyon (IN2P3-CNRS/Université), F-69622 Villeurbanne Cedex, France*
[7]*Nuclear Institute for Physics and Nuclear Engineering, Bucharest, Romania*
[8]*Dipartimento di Scienze Fisiche, Univ. di Napoli, I-80126 Napoli, Italy*
[9]*Conservatoire National des Arts et Métiers, F-75141 Paris Cedex 03, France*

(Received 28 September 2000; published 20 February 2001)

Intermediate velocity emissions of light charged particles are studied for the Ar+Ni system at 95*A* MeV. Experimental parallel velocity and transverse energy distributions are compared to those of a calculation based on intranuclear cascades followed by percolation and evaporation steps. The trends of the distributions are very similar, confirming the importance of prompt emissions in the experimental data.

DOI: 10.1103/PhysRevC.63.034612 PACS number(s): 25.70.−z, 24.10.−i

I. INTRODUCTION

Heavy ion collisions at intermediate energies (between ~30 and ~100 *A* MeV) have revealed a lot of peculiar phenomena, expectedly arising from the transition between the low energy regime where the mean field is a predominant feature and the high energy domain where two-body collisions are prevalent. Above ~200*A* MeV, the mean field is not strong enough to maintain cohesion for a sufficient time. Then, fusion as well as the binary deep inelastic process is inhibited. This leaves room for the so-called participant-spectator scenario where in the outgoing channel two rather cold projectile and target remnants are accompanied by a hot piece of nuclear matter between them (the participant zone or fireball [1]). In the intermediate energy regime, where exotic phenomena are expected because of the proximity to the Fermi energy, numerous experimental studies have been carried out. Predominance of binary collisions or the onset of the participant-spectator mechanism were claimed without indisputable evidence [2].

For the presently studied system Ar+Ni at 95*A* MeV [3,4] as well as for neighboring ones [2] or heavier ones [5–9], a rather large contribution of a binary scenario is indeed observed. However, deviations from a pure binary picture have been predicted theoretically [10] and indeed quite a few intriguing features cannot be cast in this scenario [11,12]. (How can exchanges of nucleons simultaneously lead to high excitation energy and small net mass transfer, and yet leave each partner in thermal equilibrium?) In particular the estimated number of particles between the two main fragments and their mean transverse energies [13] are waiting for a satisfactory theoretical interpretation. Indeed the yield of this intermediate velocity emission relative to the total mass of the system appears independent of the bombarding energy but is strongly dependent on the violence (geometry) of the collision [13–15]. Mechanisms like neck formation and rupture between the two fragments, extreme deformation for one of them, formation of hot spots, etc., have been proposed to explain this peculiarity. This could alternatively be interpreted as the memory of the high energy regime where the participant zone is thought to be separated from the two spectators. Another interesting aspect is provided by the mean transverse energy of these intermediate velocity emissions. It is much larger than the one of those particles which are confidently identified as evaporated from the projectile and targetlike fragments. This could be interpreted as a third intermediate source (fireball) hotter than the two main spectator remnants. The apparent geometrical influence reinforces the suspicion, if not the conviction, that the regime of high energy has already settled [16,17].

The intranuclear cascade (INC) model is the simplest microscopic model of the nucleus-nucleus interaction that, at relativistic energy [18–21], yields the participant-spectator scenario as a result [22]. This model showed good agreement with the Bevalac data in the 1980s and has recently received

*Deceased.

†Present address: CEA, DRFC/STEP, CE Cadarache, 13108 Saint-Paul-lez-Durance, France.

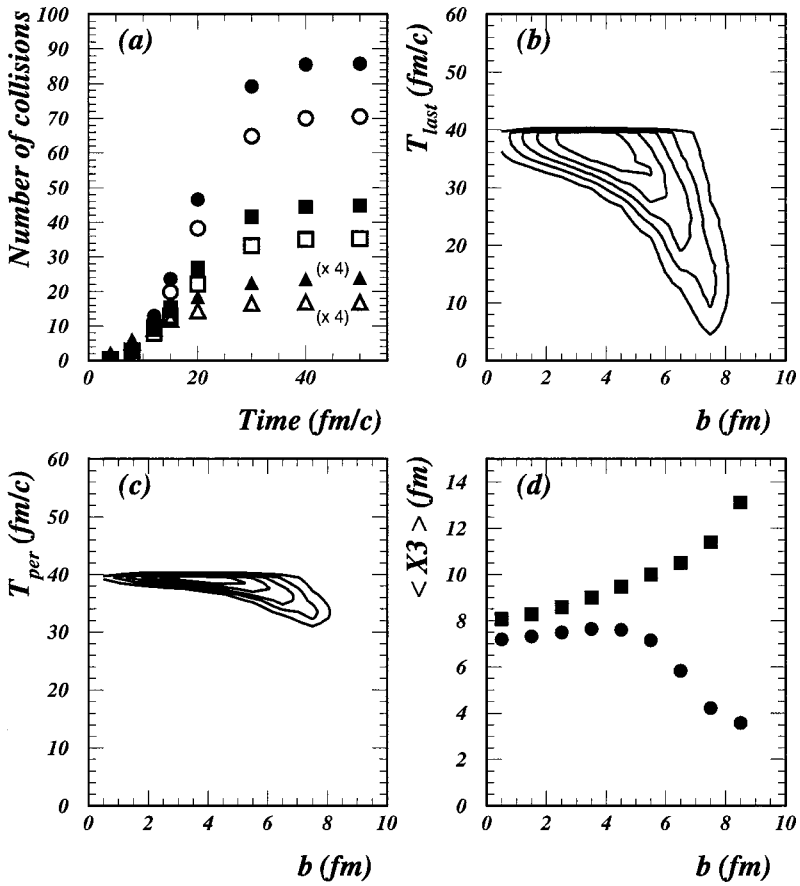

FIG. 1. Intranuclear calculation ingredients. (a) Cumulative number of hadron-hadron collisions with (open symbols) and without (solid symbols) a simulated potential for different impact parameters [$b=1$ fm (circles), 4 fm (squares), and 7 fm (triangles)] as a function of time. The results for $b=7$ fm have been multiplied by 4. (b) Time of the last collision and (c) percolation time as a function of the impact parameter. Contours in (b) and (c) are equidistant. (d) Mean position (parallel to the beam direction; the origin is the target) of the noninteracting projectile nucleons at t_{per} (squares) and t_{last} (circles) (see text).

renewed interest with the advent of accelerator driven system projects [23,24]. In this paper we will apply the nucleus-nucleus INC plus percolation model of Ref. [25] followed by an evaporation code [26] to the Ar+Ni measurements at 95*A* MeV. Although, at this incident energy, the validity of the INC model is *a priori* marginal, a comparison of the overall behavior of the data with this model can provide a useful tool to evaluate the departure from a pure binary scenario. In Sec. II the INC-percolation-evaporation model will be presented. Typical results of the INC-percolation approach are presented in Sec. III. An extensive comparison between data and calculations will be given and discussed in Sec. IV. Finally, Sec. V contains our conclusions.

II. INTRANUCLEAR CASCADE-PERCOLATION-EVAPORATION MODEL

A. Brief description

In this study we use the INC+percolation model of Ref. [25], based on the Liège INC model, first developed in Ref. [21], including also a recently improved parametrization of the nucleon-nucleon interaction cross sections as described in Refs. [27,28]. Most of the details on the Liège INC model are given in [21] and references cited therein. It is sufficient here to describe the main points. The model includes pion and delta production as well as an isospin degree of freedom. At the beginning ($t=0$), nucleons inside each nucleus are randomly positioned in a sphere of radius $1.12A^{1/3}$ fm (where A is the nucleus mass) and in a momentum sphere of radius $P_F=235$ MeV/c. The Fermi motion of any nucleon is frozen up to its first collision. The impact parameter (b) of the collision is randomly chosen in a disk of radius equal to the sum of the radii of the two nuclei. The calculation uses relativistic kinematics. Particles move along straight line trajectories until two of them reach their minimum distance of approach, d_{min}. Whether they collide or not is governed by a comparison of the total collision cross section with πd_{min}^2. The Pauli principle is applied to forbid final states already occupied. The blocking factor relies on phase space occupation probabilities inside a reference volume centered around each particle in the final state. This reference volume is the direct product of a sphere in ordinary space of 2 fm radius and a sphere in momentum space of 200 MeV/c radius. Soft collisions, i.e., with a c.m. energy smaller than 35 MeV, are suppressed. They would be forbidden by the Pauli principle to a very large extent, but this procedure considerably shortens the computation time. The potential energy of the nucleons in the nuclei is neglected. The absence of a potential, avoiding a treatment of collisions for off mass shell nucleons, is justified at high bombarding energies. At this bombarding energy, the potential energy will be restored in an approximate manner, as explained in the following subsection.

All the particles are followed in time up to a stopping time t_{stop} discussed below. Since colliding nuclei are treated as a cloud of nucleons, fragments are not naturally defined at

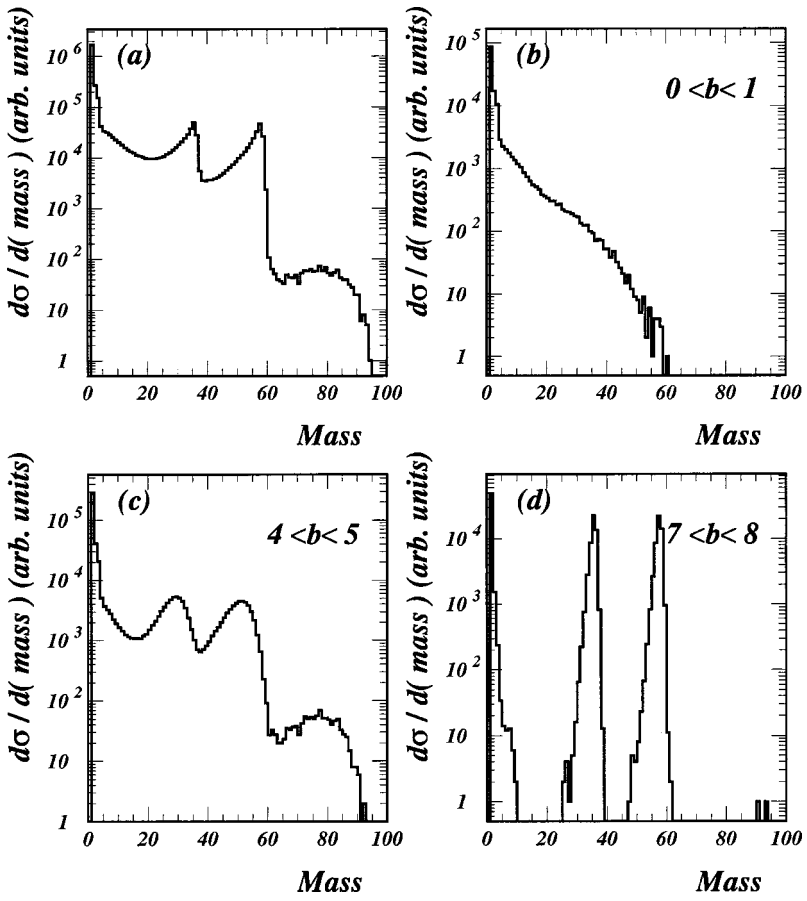

FIG. 2. Results of the intranuclear cascades and the percolation procedure. Mass distributions for all events (a), for central (b), midcentral (c), and peripheral (d) collisions.

the stopping time. A percolation procedure is used to construct residual fragments. The spatial distribution is considered and two nucleons are attributed to the same cluster if their relative distance is smaller than a chosen percolation distance d_{cut}. This requires the construction of a minimum spanning ''tree'' [29] based on the links (relative distances) between nucleons. Links larger than the percolation distance are cut out. Nucleons which remain linked together form a cluster.

Percolation generates free nucleons, light composite particles, and excited fragments. The excitation energy of the clusters can be evaluated by looking at the internal motion in their center of mass frame. It is defined as the difference between the total energy of the nucleons inside a cluster and the sum of the mass energy of the constituents. This excitation energy has to be evacuated by means of an afterburner. The evaporation code of Dresner [26] has been chosen for that purpose. It is commonly employed in transport code systems like HETC and LAHET [30,31] and calculates the statistical decay of the fragments, following Weisskopf theory [32], through light particle (n, p, d, t, ^{3}He, ^{4}He) emission. Angular momentum is neglected. Level density parameters are taken from Ignatyuk *et al.* [33]. Instead of the standard evaporation formula, the code implements the Fermi breakup [34] model for the deexcitation of light fragments with mass number between 5 and 21.

In the next subsections, we give more details of the model of Ref. [25].

B. Potential restoration

In order to partly restore the effect of the potential well felt by nucleons inside nuclei, a feature that can be of importance at the relatively low bombarding energy studied here, we follow the procedure of Ref. [35], which has proved to be quite successful for the analysis of a vast body of data in the (250–800)A MeV range. Since the origin of any colliding nucleon is known (target or projectile), its energy, relative to its emitter, can be determined after any nucleon-nucleon collision. It is compared to a value V. This ''potential'' energy, 32 MeV, was determined in a somewhat *ad hoc* manner in Ref. [35], but it is close to the average (over all the nucleons of a nucleus) energy needed for a nucleon to escape from the potential well. Nucleons more energetic than V can ''escape,'' with an energy lowered by V; otherwise they ''reintegrate'' their parent nucleus waiting for a possible new collision.

This procedure satisfactorily describes the kinetic energy of the free nucleons [35]. It however introduces a violation of energy conservation in the model calculation. This can be cured, considering that the energy lost in this procedure is mainly recovered under the form of the excitation energy of the clusters. It is reasonable that this extra excitation energy can be attributed to the nucleons that have been hit but that did not have enough energy to escape their parent nucleus. Let ΔE be the energy lost in the procedure described above. We then correct the excitation energy of a fragment f by a quantity (δE) given by $(Nin_f/Nin_{tot})\Delta E$ where Nin_{tot} is

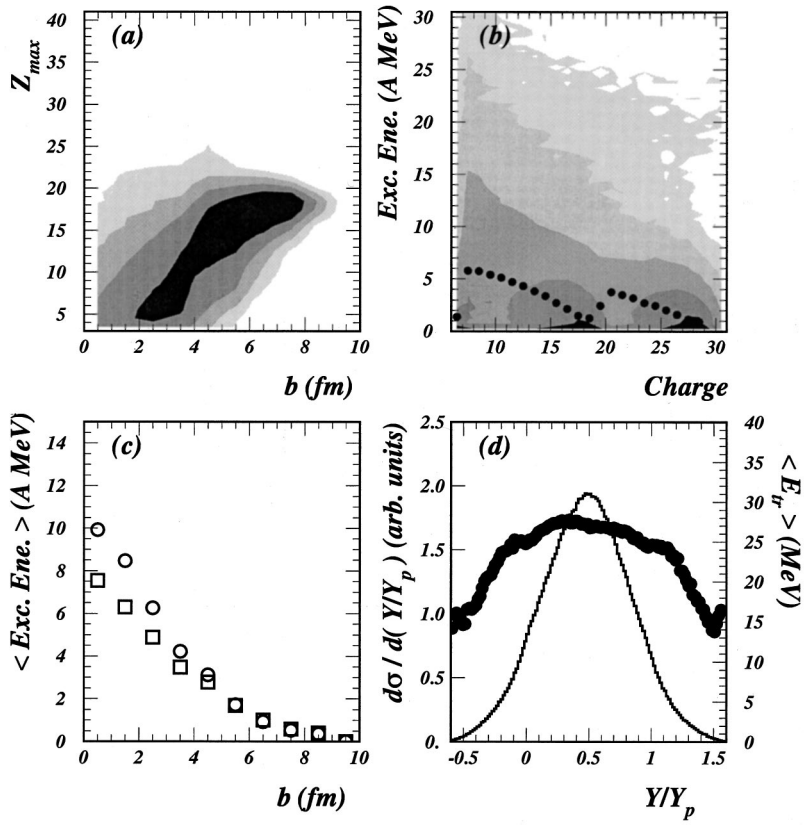

FIG. 3. Results of the intranuclear cascades and the percolation procedure. (a) Z_{max} (charge of the largest fragments in the forward hemisphere) versus the impact parameter. (b) Excitation energy of the remnants as a function of their charge (points are the mean values). There is a factor of 7 between each contour level in the bidimensional plots (a) and (b). (c) Mean excitation energies for the QP (circles) and the associated QT (squares) residues ($Z_{max}>6$) as a function of the impact parameter. (d) Proton rapidity distribution (left scale, histogram) and mean transverse energy (right scale, points).

the total number of nucleons not able to escape in the whole system, Nin_f the nucleons included in a fragment f which were not able to escape. This correction is applied to fragments of charge greater than 6. This procedure restores energy conservation in the model. It allows us to treat in a reasonable, albeit crude, manner the potential energy effects while keeping the simplicity of the cascade approach. Correcting the excitation energy rather than the kinetic energy of the fragments is justified in some sense by the fact that the main momentum flow is governed by collisions, accurately described by the cascade model.

C. Transition from INC to percolation

This is a somewhat subtle question. In the version of the Liège INC model for nucleon-nucleus collisions (where a static potential well is introduced), the stopping time has been parametrized [28] as a function of target mass, incident energy, and impact parameter using criteria based on the evolution of various variables with time. Namely, the excitation energy of the remnant (naturally defined by the nucleons remaining in the volume of the potential well), emission anisotropy, and saturation of the cumulative numbers of collisions or of escaping particles were studied. Changes of behavior were observed at about the same time, so defining the

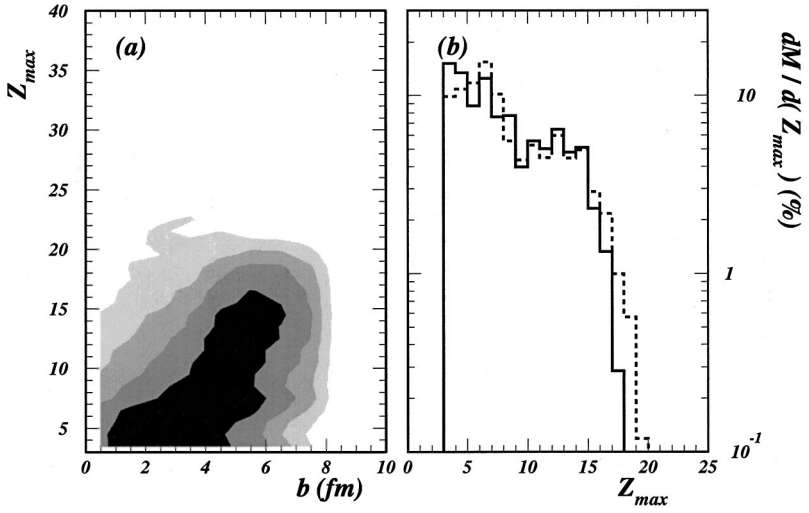

FIG. 4. Results of the calculations after intranuclear cascades+percolation+evaporation procedure and filtering. (a) Z_{max}, charge of the largest fragments in the forward hemisphere, versus the impact parameter b. There is a factor of 7 between each contour level. (b) The calculated Z_{max} differential multiplicity in percentage (dashed line histogram) is compared to the experimental one (solid line histogram).

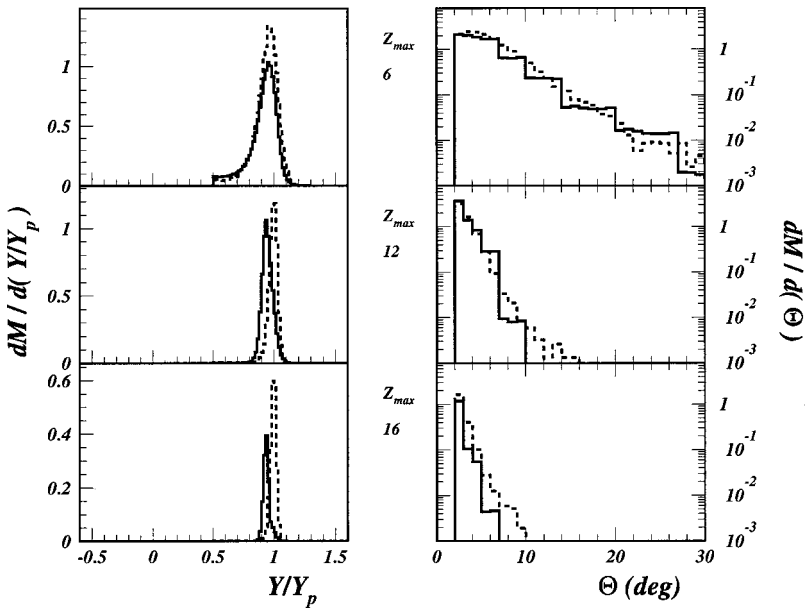

FIG. 5. Rapidity (left panel) and angular (right panel) distributions for $Z_{max}=6$, 12, and 16. Solid-line histograms are the data and dashed-line histograms the calculations. The steps in the experimental angular distributions are due to the angular segmentation of the detector. The normalization is the same as in Fig. 4.

stopping time, t_{stop} rather consistently. In our case, the stopping time is determined in a similar manner. Figure 1(a) shows, for the Ar+Ni system at 95*A* MeV, the evolution of the cumulative number of colliding baryons versus the development time of the intranuclear cascade for different impact parameters. One can notice that, at a given time, the number of collisions increases with centrality of the collisions. However, one observes also a saturation around 30–40 fm/c, for all impact parameters. Adopting our method to take into account the binding potential does not change the picture very much. The number of colliding baryons (open symbols) is slightly smaller because collisions are sometimes inhibited for low energy nucleons.

According to this criterion, the stopping time has been set to 40 fm/c. In Ref. [25] the percolation is applied to the configuration at the latest collision before the stopping time. The time t_{last} at which this latest collision occurs is given in Fig. 1(b) as a function of the impact parameter. In Ref. [25], the percolation distance d_{cut} is chosen to be 2 fm, a reasonable value in regard to the average distance between nucleons in ordinary nuclear matter. Here we elaborate a bit on these choices, inspired by the observation that we are facing quite different configurations according to the impact parameter. We consider the possibility of performing the percolation at a time t_{per} later than t_{last}. For small impact parameters, the configurations are rather homogeneous and close to a spherical geometry. The collision process is almost over [see Figs. 1(a) and 1(b)]. In such conditions, there is an approximate correlation between d_{cut} and t_{per} leading to roughly the same fragmentation pattern: an increase of t_{per} can be compensated by an increase of d_{cut},[1] as explained in Refs. [25,35]. We checked this property for the system under consideration. For very peripheral collisions, t_{last} is rather small, and at this time, the quasiprojectile and the quasitarget are almost touching each other, with perhaps one or two nucleons in between. A straight application of percolation on such a configuration leads to a spurious ''fusionlike'' event as the minimum spanning ''tree'' recognizes a link between the two main clusters. Since quasiprojectile, quasitarget, and nucleons in between have rather different velocities (in the longitudinal direction), there are no d_{cut}-t_{per} correlations for this case. This property could be exploited: adopting a t_{per} larger than t_{last} propagates the fragments[2] and the nucleons further and separates the two big fragments from each other. For not too large impact parameters (midperipheral collisions), the situation is a little bit different: there are still two large fragments not too far away from each other with nucleons and perhaps one or two light clusters in between. Increasing t_{per} to achieve a good separation of the big clusters may dissociate the light ones. This can be circumvented by increasing d_{cut}. These considerations suggest that a compromise can be reached by an appropriate *b*-dependent choice of t_{per} and d_{cut}. Similar considerations and similar choices are made in Ref. [35]. Here, we chose $t_{per}=t_{last}+0.75(t_{stop}-t_{last})$ and d_{cut}^2 varying linearly with the impact parameter from 3 fm^2 for central collisions to 8 fm^2 for peripheral ones. The values of t_{per} are shown in Fig. 1(c). These adjustments allow one to have the mean position of the noninteracting nucleons of the projectile, relative to the target position, at the percolation time, to vary slightly and monotonically with the impact parameter. They thus allow one to perform percolation in largely homogeneous conditions. This is illustrated in Fig. 1(d) where the mean longitudinal position of the noninteracting projectile nucleons at t_{last} (circles) and t_{per} (squares) is presented as a function of the impact parameter. This procedure can be interpreted as a

[1]This exactly holds for a self-similar flow, i.e., when the particles have a radial outward velocity proportional to their distance from the center of the system.

[2]One has to remember that nucleons inside the quasiprojectile and the quasitarget have practically not interacted. The Fermi motion is thus frozen inside these objects and they thus move as a whole.

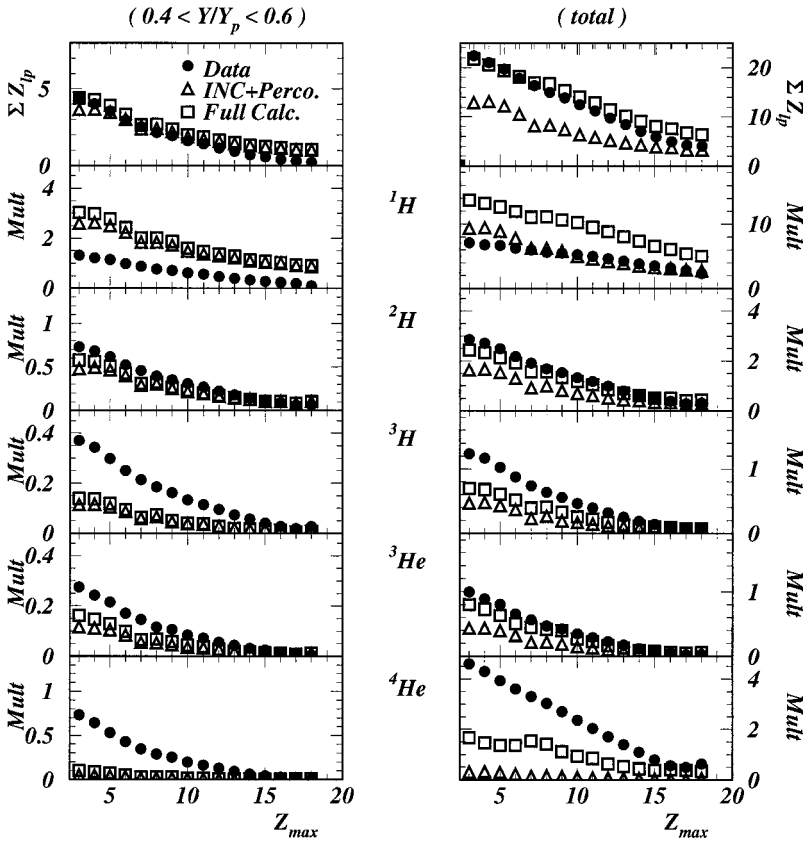

FIG. 6. Total charge and multiplicities of different light charged particles integrated over the midrapidity region ($0.4 \leqslant Y/Y_p \leqslant 0.6$) in the left panel and integrated over the whole rapidity range in the right panel as a function of Z_{max}. The solid circles represent the data, the open triangles are the results of the cascade+percolation steps, and the open squares are the results of the full calculation (cascade+percolation +evaporation). Statistical error bars are smaller than the symbol sizes.

compensation required by percolation being performed in ordinary space only and not in phase space.

III. RESULTS OF THE INC+PERCOLATION CALCULATION

The basic results of the INC + percolation are displayed in Figs. 2 and 3, for the Ar+Ni system. The mass distribution shown in Fig. 2(a) exhibits a small contribution of fusion events at masses ~ 80 and target ($A=58$) and projectile ($A=36$) remnants. In (b), (c), and (d) the mass distributions are depicted for three different impact parameters. For central collisions we observe a continuously decreasing distribution with mass, while for midcentral reactions, the reminiscence of the quasiprojectile (QP) and quasitarget (QT) fragments begins to appear and is finally predominant for peripheral collisions. Most of fusion events for midperipheral collisions are spurious and translate the fact that the procedure mentioned above is not entirely efficient. Since the contribution of these events is small (less than 1%), they will simply be rejected in the rest of the analysis. Figure 3(a) shows a calculated bidimensional distribution Z_{max} impact parameter, Z_{max} being the largest fragment charge with a rapidity larger than half the projectile rapidity ($Y_{Z_{max}} \geqslant Y_p/2$). One can observe a gentle relaxation in the mass of the quasiprojectile with decreasing impact parameter down to 4 fm followed by a faster falloff.

Calculated excitation energies per nucleon are shown in Fig. 3(b), as a function of the fragment charge. Mean values (points) are superimposed. The two major contributions correspond to projectile ($Z \leqslant 18$) and target remnants ($Z \leqslant 28$). One observes rather low values, increasing with decreasing remnant mass. As expected this variation illustrates the increasing relaxation when the mass of the primary fragment moves off the one of the original nucleus it is coming from. In Fig. 3(c) the mean excitation energies for the QP (circles) and QT (squares) residues, in coincidence, are shown according to the impact parameter. The identification of the remnant fragments ($Z_{max} > 6$) as QP and QT have been done according to a selection on velocity criteria: $Y/Y_p > 0.5$ for QP and $Y/Y_p < 0.5$ for QT. For midperipheral and peripheral collisions, the temperatures of the QP and QT residues are roughly equal. The situation seems to evolve towards an equal sharing of the excitation energy between QP and QT as the collisions are becoming more and more central. However, the identification of QP and QT becomes rather difficult at small impact parameters.

After intranuclear cascade and percolation, the outgoing channel is composed of fragments and free nucleons, production of pions being marginal at the studied energy. Free nucleons can be viewed as the so-called preequilibrium particles. Some characteristic features of the free protons are shown in Fig. 3(d). The histogram represents their rapidity distribution in the laboratory frame, normalized to the projectile rapidity, integrated over all impact parameters. It is peaked at the reduced rapidity equal to 0.5, as it would be in nucleon-nucleon collisions with the same kinematics. Because of multiple collisions and Fermi motion, the spectrum extends significantly beyond the target and projectile region ($Y/Y_p = 0$ and 1, respectively). This extension is in qualitative agreement with the velocity distribution of dynamically emitted particles predicted by a semiclassical transport

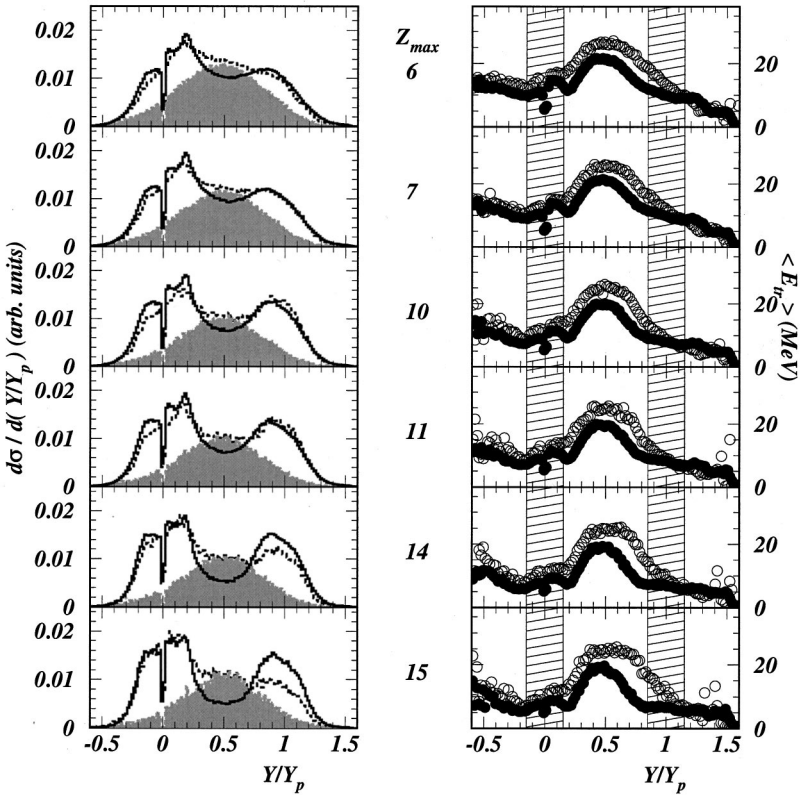

FIG. 7. Proton characteristics for different Z_{max} values. Left: proton reduced rapidity distributions. The data are indicated by the solid-line histograms, the results of the full calculation by the dashed-line histograms. The solid-grey histograms correspond to the cascade+percolation stage. Right: proton mean transverse energy versus Y/Y_p. Data are shown by solid symbols and calculations by open symbols. The QP and QT regions are denoted by shaded areas.

model [10]. The points in Fig. 3(d) show the variation of the mean transverse energy ($E_{tr}=m_0c^2[\sqrt{1-\gamma^2\beta_\perp^2}-1]$, where γ is the Lorentz factor, $\beta_\perp$ the perpendicular reduced velocity, and m_0 the mass of the particle) versus the reduced rapidity. In nucleon-nucleon collisions with the same kinematics one expects a maximum value of $\langle E_{tr}\rangle$, equal to $E/4$ where E is the incident energy. In the nucleus-nucleus collisions considered here, the maximum value is somewhat larger ($\sim$27 instead of 23.75 MeV). This presumably comes from a depletion of the free nucleon population in the vicinity of the c.m. velocity, i.e., close to $Y/Y_p\approx 0.5$ and the transverse momentum $p_\perp\approx 0$. There are at least two reasons for this: the Pauli principle, as the two original Fermi spheres are slightly overlapping, and the percolation procedure which tends to aggregate more low $p_\perp$ nucleons.

IV. COMPARISON WITH EXPERIMENTAL DATA

Experimental data were obtained with INDRA [36], a 4π multidetector for charged particles. The experiment was performed at the GANIL facility which provided an ^{36}Ar beam of $3-4\times 10^7$ particles per second at 95A MeV bombarding a self-supporting 193 μg/cm^2 thick ^{58}Ni target. A minimum bias trigger required a fourfold event. Charge identification was achieved up to the projectile charge in the forward hemisphere. Hydrogen and helium isotopes were separated for detection angles from 3° to 176°. For spectra presented here, software energy thresholds were fixed at 2A MeV for hydrogen isotopes and 1A MeV for helium isotopes to homogenize the data in the whole detector. Angles were chosen randomly inside the limiting angles of each ring of the detector.

Results of the full calculation (INC+percolation +evaporation) are filtered taking into account the geometry of the detector, the punch-through energies as well as the energy, and identification thresholds. Figure 4(a) shows the correlation between Z_{max}, the charge of the largest fragments in the forward hemisphere, and the impact parameter. As shown in Figs. 3(a) and 4(a) a fair correlation exists between Z_{max} values and the impact parameter. The decrease of Z_{max} with the impact parameter is, however, smoother in the full calculation than before evaporation. Hence, Z_{max} can be used to classify the events according to the violence of the collision. The lowest values of Z_{max} are associated with the most central processes and the values of Z_{max} near the projectile charge to peripheral interactions. Experimental and calculated fragment characteristics are compared in Figs. 4 and 5. Figure 4(b) shows the experimental (solid line histogram) and calculated (dashed line histogram) Z_{max} distributions. A reasonable agreement in shape can be observed. One can note the depletion at $Z_{max}=9$ produced by the small number of stable isotopes of this element. This effect is also visible in Fig. 4(a) where the element $Z=8$ is more populated.

In the left panel of Fig. 5 are compared the laboratory rapidity spectra for different Z_{max} values. A fair agreement is also obtained but calculated spectra show a smaller relaxation as well as a narrower width than the data. The absence of the mean field in the calculation could probably explain this discrepancy. Angular distributions for the same Z_{max} values are compared in the right panel of Fig. 5. One observes a rather good agreement for low Z_{max} values which deteriorates for peripheral collisions.

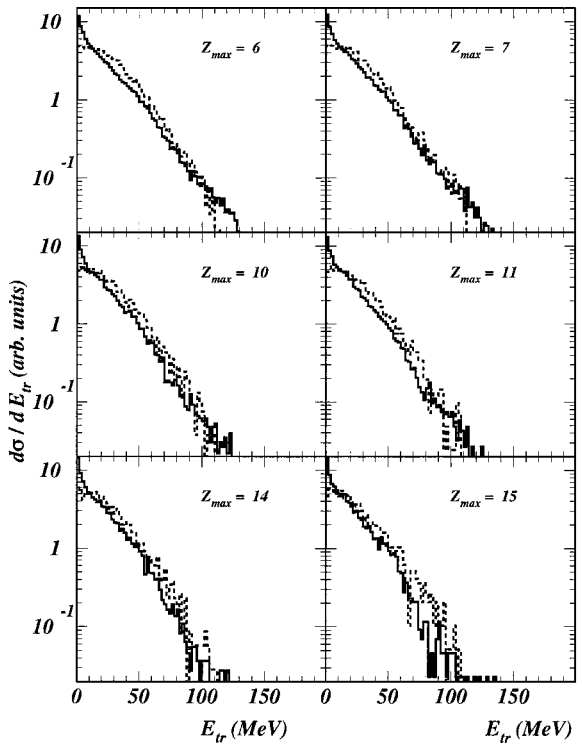

FIG. 8. Experimental (solid-line histograms) and calculated (dashed-line histograms) proton transverse energy spectra for a few selected Z_{max} values as indicated. Protons with a reduced rapidity between 0.45 and 0.55 are selected.

In Fig. 6 are presented the total charge and the multiplicities of different light charged particles integrated over the midrapidity region ($0.4 \leqslant Y/Y_p \leqslant 0.6$) (left panel) and integrated over the whole rapidity range (right panel), as a function of Z_{max}. Since the aim of this study was the understanding of the midrapidity components, we first comment on the left panel of Fig. 6. In the upper part the sums of charges (essentially light charged particles) in the region $0.4 \leqslant Y/Y_p \leqslant 0.6$ are compared. Except for the peripheral collisions (large Z_{max}) where there is a slight overestimation, the calculations agree quite well with the data. Thus this shows that the model is well suited for this particular region of interest. The individual light particle multiplicities in the midrapidity region are also compared. The calculated multiplicities are shown before and after the evaporation stage. One can notice that the evaporation step has little influence in this region. For all light particle species the predicted trend of the variation of the multiplicities versus Z_{max} follows the experimental behavior rather well. However, there is an overestimation of the proton production. One can notice that the deuteron and to a lesser extent the ^{3}He multiplicities are well reproduced. For tritons and mainly for alpha particles, the calculation underestimates the data. The same observables are compared for the full rapidity range on the right panel of Fig. 6. One still observes a good agreement for the total charge and also for the individual multiplicities. The general trend is well reproduced. One can remark that the evaporative contribution becomes rather important and that the reproduction of the data is of the same quality as for the midrapidity region. The prompt component (before evaporation) varies from 30% to 5% of the total system charge going from central to peripheral collisions. The excess of protons is undoubtedly related to the underestimation of alpha particle yields. It seems that too many free protons are left after the percolation, since, after this stage already, theoretical predictions reach the experimental values. Hence we could infer that percolation does not build enough clusters. A similar observation was done in a recent work [37] using the intranuclear cascade code ISABEL [19] complemented by a coalescence procedure in momentum space. This study, restricted to the midrapidity component, shows also difficulties in building enough clusters. The treatment of the aggregation process is still an unsolved problem on which further theoretical works are needed. Another part of the discrepancies for ^{4}He could be due to the evaporation code itself which is known to underestimate alpha production for light systems [38]. Since the production of heavier particles is more sensitive to the angular momentum, the neglect of it could also explain part of the discrepancy. The prediction of the relative production rate can depend on the various default parameters used in the evaporation code which could not be very well tuned for the present large spread of excitation energies in residual nuclei. Kinematical properties could be a better test of the potential of the present model.

In the left panel of Fig. 7 the calculated (dashed-line histograms) proton rapidity distributions are compared to the experimental data (solid-line histograms) for some Z_{max} values. The spectra, calculated in the laboratory frame, are normalized to the number of protons associated with each residue. The experimental shape is fairly well reproduced with, however, a tendancy to slightly overestimate the midrapidity component. The largest discrepancies arise for the highest Z_{max} values, where the predicted yield in the midrapidity region is too large while the QP component is underestimated. These effects could be partly due to the difficulty of our model to reproduce the strong forward peaking of the QP remnant for these peripheral collisions. The contribution from pure intranuclear cascades (solid histograms) fills up nicely the midrapidity region and extends well above the projectile and below the target bumps. This also agrees quite nicely with the results of the three source analysis performed in Ref. [14] for the same system.

The mean transverse energy (right panel of the Fig. 7) is an interesting variable which clearly signals the occurrence of midrapidity emission [13]. The calculations (open symbols) exhibit as the data (solid symbols) the presence of a plateau in the QP and QT regions and a large peak at midrapidity. The $\langle E_{tr} \rangle$ values remain constant as a function of Z_{max} in the midrapidity region but increase in the QP and QT regions (shaded area in right panel of the Fig. 7) from 5 MeV to 10 MeV for Z_{max} decreasing from 15 to 6. This variation in the QP and QT regions, which could be interpreted as a higher energy transfer when Z_{max} diminishes, is well reproduced by the calculation. This increase could also be due to the growing contamination of the midrapidity contribution in this region for the smallest Z_{max} values. The global trend of the $\langle E_{tr} \rangle$ curve is well accounted by the calculation. However, the peak at midrapidity is located at a somewhat higher

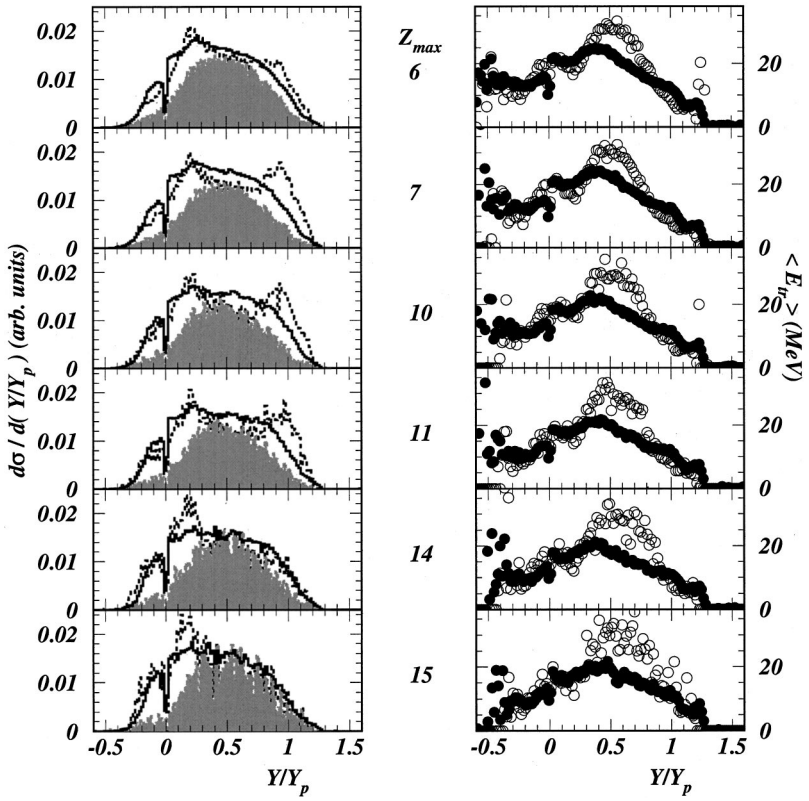

FIG. 9. Deuteron characteristics for different Z_{max} values. Left: deuteron reduced rapidity distributions: data (solid-line histograms), full calculation (dashed-line histograms), and before evaporation (solid histograms). Right: deuteron mean transverse energy versus Y/Y_p. Data are shown by solid symbols and calculations by open symbols.

reduced rapidity and the mean value is too large (25 MeV instead of 20 MeV) especially for the most peripheral collisions. The use of mean values could be an easy way to summarize the data but a more significant comparison is presented in Fig. 8 where the proton transverse energy spectra in coincidence with different Z_{max} fragments are shown. Only the region of midrapidity ($0.45 \leqslant Y/Y_p \leqslant 0.55$) for protons is presented. The normalization has been done on the total content of each spectrum. The slopes at high energies are nicely reproduced, showing that the present calculations are able to simulate quite well the characteristics of the midrapidity particles. Only the low energy region below 10 MeV is under predicted. This part of the spectra could also be populated by particle emission from equilibrated large remnants. The too small theoretical dissipation could be responsible for this discrepancy; the QP and QT remnants are predicted to be too far apart in the velocity space in our model, and thus this region is not sufficiently populated by their evaporation.

In Fig. 9, deuteron rapidity distributions in the laboratory frame (left panel) and mean transverse energies (right panel) are presented. The agreement between experimental (solid-line histograms) and calculated (dashed-line histograms) rapidity distributions, although less satisfactorily than for protons, is good. The midrapidity region is satisfactorily reproduced but there is an overestimation by the calculations of the evaporative part in the QP region which is less apparent in the QT region for the most central collisions. Concerning transverse energies, the same discrepancy as for protons is observed. The mean calculated values at intermediate velocity are too high. One also notices that the excess of the deuteron evaporation lowers the mean predicted transverse energy in the QP region. However, the general kinematical trend and the multiplicities (Fig. 6) are well reproduced. Experimental transverse energy spectra are more shifted towards the target side than for protons while the calculations still predict the bump location at midrapidity. Processes other than nucleon-nucleon collisions followed by percolation could contribute to this region like nucleon-cluster scatterings [39]. This shift is more pronounced for heavier light charged particles not shown here. For these particles, the calculations significantly underestimate the total yield, as shown in the left part of Fig. 6.

V. SUMMARY

We have studied some aspects of Ar+Ni collisions at 95*A* MeV, a bombarding energy regime where both binary collisions and participant-spectator processes are claimed to compete. In this paper, we did not attempt a thorough description of the data with a model embodying some mixtures of the two scenarios. Instead, we adopted the following methodology: take a microscopic approach which encompasses the participant-spectator scenario, look at the predictions of the model, and try to assess and interpret the possible deviations. The microscopic approach adopted here, namely, the intranuclear cascade, should of course be supplemented by other models, here a percolation and an evaporation step, to account for the soft processes taking place at the end of any collision process. We compared the predictions of our theoretical model with two kinds of observables: those concerning the heavy fragments and those concerning light particles in the intermediate velocity range.

The model describes reasonably well the charge distribution of the largest projectilelike fragment and the rapidity

and angular distributions of these fragments. Slight deviations of the theoretical predictions from the data could indicate that those observables cannot be fully described by simple interactions, dictated by geometry as in the INC + percolation approach. These features are commonly understood as coming from nucleons behaving collectively inside the projectilelike fragments, owing to the action of the mean field. The observed agreement is gratifying. It suggests that already at the present bombarding energy, the nucleon-nucleon collisions play a more crucial role than the mean field especially for the central collisions.

A special emphasis has been put on light particle emission in the midrapidity region since the physics of the participants is well suited to the treatment by the intranuclear cascades. The kinematics properties of this region which presumably cannot be explained by treatments assuming thermalized emission from the projectile and target remnants are well reproduced by the present model. This shows that its simple physics input is able to describe the properties of the particles emitted in the velocity region between the target and the projectile remnants. Moreover, our theoretical model is able to describe correctly the evolution of these observables with the charge of the projectilelike fragment.

A systematic discrepancy between the theoretical and the experimental locations of the maximum of the mean transverse energy is observed and could point towards the presence of an extra contribution beyond the dominant nucleon-nucleon collisions. In fact, even in this intermediate velocity emission, the dynamics cannot be reduced entirely to the simple INC picture. More sophisticated transport models are probably necessary to bring further quantitative agreements but they need at least to incorporate the simple ingredients present in the intranuclear cascade model.

[1] J. Gosset, H. H. Gutbrod, W. G. Meyer, A. M. Poskanzer, A. Sandoval, R. Stock, and G. D. Westfall, Phys. Rev. C **16**, 629 (1977).
[2] R. Dayras *et al.*, Nucl. Phys. **A460**, 299 (1986).
[3] M. F. Rivet *et al.*, Phys. Lett. B **388**, 219 (1996).
[4] Y. G. Ma *et al.*, Phys. Lett. B **390**, 41 (1997).
[5] C. P. Montoya *et al.*, Phys. Rev. Lett. **73**, 3070 (1994).
[6] J. Tõke *et al.*, Nucl. Phys. **A583**, 519 (1995).
[7] J. F. Lecolley *et al.*, Phys. Lett. B **354**, 202 (1995).
[8] E. Plagnol *et al.*, Phys. Rev. C **61**, 014606 (1999).
[9] F. Bocage *et al.*, Nucl. Phys. **A676**, 391 (2000).
[10] Ph. Eudes, Z. Basrak, and F. Sébille, Phys. Rev. C **56**, 2003 (1997).
[11] Y. Larochelle *et al.*, Phys. Rev. C **55**, 1869 (1997).
[12] J. E. Sauvestre *et al.*, Phys. Lett. B **335**, 300 (1994).
[13] T. Lefort *et al.*, Nucl. Phys. **A662**, 397 (2000).
[14] D. Doré *et al.*, Phys. Lett. B **491**, 15 (2000).
[15] Ph. Buchet, Ph.D. thesis, Université de Caen, 1999.
[16] R. G. Stokstad *et al.*, Comments Nucl. Part. Phys. **13**, 231 (1984).
[17] D. Lebrun *et al.*, Phys. Lett. B **223**, 139 (1989).
[18] K. Chen, Z. Fraenkel, G. Friedlander, J. R. Grover, J. M. Miller, and Y. Shimamoto, Phys. Rev. **166**, 949 (1969).
[19] Y. Yariv and Z. Fraenkel, Phys. Rev. C **20**, 2227 (1979).
[20] V. D. Toneev and K. K. Gudima, Nucl. Phys. **A400**, 173c (1983).
[21] J. Cugnon, Phys. Rev. C **22**, 1885 (1980).
[22] J. Cugnon and S. E. Koonin, Nucl. Phys. **A355**, 447 (1981).
[23] C. D. Bowman *et al.*, Nucl. Instrum. Methods Phys. Res. A **320**, 336 (1992).
[24] C. Rubbia *et al.*, Report No. CERN/AT/95-44(ET), 1995.
[25] J. Cugnon and C. Volant, Z. Phys. A **334**, 435 (1989).
[26] L. W. Dresner, Oak Ridge Report No. ORNL-TM-196, 1962.
[27] J. Cugnon, S. Leray, E. Martinez, Y. Patin, and S. Vuillier, Phys. Rev. C **56**, 2431 (1997).
[28] J. Cugnon, C. Volant, and S. Vuillier, Nucl. Phys. **A620**, 475 (1997).
[29] E. W. Dijkstra, Numer. Math. **1**, 269 (1959); J. Dorfan, Z. Phys. C **7**, 349 (1981).
[30] T. W. Armstrong and K. C. Chandler, Radiation Shielding Information Center, HETC Monte-Carlo Nucleon-Meson Transport Code, Report No. CCC-178, ORNL, 1977; Nucl. Sci. Eng. **49**, 110 (1972).
[31] R. E. Prael and H. Lichtenstein, Los Alamos National Laboratory Report No. LA-UR-89-3014, 1989.
[32] V. F. Weisskopf, Phys. Rev. **52**, 295 (1937).
[33] A. V. Ignatyuk, G. N. Smirenkin, and A. S. Tishin, Yad. Fiz. **21**, 485 (1975) [Sov. J. Nucl. Phys. **21**, 255 (1975)].
[34] E. Fermi, Prog. Theor. Phys. **5**, 1570 (1950).
[35] G. Montarou *et al.*, Phys. Rev. C **47**, 2764 (1993).
[36] J. Pouthas *et al.*, Nucl. Instrum. Methods Phys. Res. A **357**, 418 (1995).
[37] P. Pawłowski *et al.*, Eur. Phys. J. A **9**, 371 (2000).
[38] M. Enke *et al.*, Nucl. Phys. **A657**, 317 (1999).
[39] A. Hürstel *et al.*, in *Proceedings of the XXXVIIIth International Winter Meeting on Nuclear Physics*, Bormio, Italy, 2000, edited by I. Iori [Ric. Sci. Ed. Perm. Suppl. **116**, 587 (2000)].